Predicting the time-evolution of CO_2 saturation through a combination of rock physics and full waveform inversion

Qi Hu[1], *Dario Grana*[2] *and Kristopher A. Innanen*[1]
[1] *Dept. of Geoscience, CREWES Project, University of Calgary;*
[2] *Dept. of Geology and Geophysics, School of Energy Resources, University of Wyoming.*

SUMMARY

Carbon capture and storage is a viable greenhouse gas mitigation technology. Monitoring of CO_2 should, in addition to locating the plume, provide quantitative information on CO_2 saturation. We propose a full waveform inversion (FWI) algorithm for the prediction of the spatial distribution of CO_2 saturation from time-lapse seismic data. The methodology is based on the application of a rock-physics parameterized FWI scheme that allows for direct updating of reservoir properties. We derive porosity and lithology parameters from baseline data and use them as input to predict CO_2 saturation from monitor data. The method is tested on synthetic time-lapse data generated for the Johansen formation model. We show that both the errors in baseline model estimates and the errors in monitor data could compromise the recovered CO_2 saturation model. We propose to use the Tikhonov regularization that encourages solution smoothness to help the convergence towards geologically realistic models.

INTRODUCTION

An important technology supporting reduction of greenhouse gas emissions is the geological storage of carbon dioxide, or CO_2 (Davis et al., 2019; Ringrose, 2020); for instance, deep saline aquifers have been identified as promising sites for CO_2 storage. A critical enabler for CO_2 will be reliable and low-cost monitoring of injection and storage in the subsurface. Time-lapse seismic surveys provide a monitoring mode in which migration and distribution of the injected CO_2 can be tracked, and leakage problems if any can be identified (Ghosh et al., 2015). Ideally, for reliable conformance verification, quantitative estimates/maps of CO_2 saturation would be produced by such technology, to be compared against reservoir modeling predictions (Dupuy et al., 2021).

Qualitative interpretation of CO_2 from analysis of amplitude changes and time shifts on post-stack seismic images is generally insufficient to understand detailed reservoir conditions (Alemie, 2017). Moreover, multiple reflections, interference effects such as tuning, and attenuation introduce ambiguities into seismic images which impede estimation of CO_2 position (Queißer and Singh, 2013b). A promising approach to address these issues involves seismic full waveform inversion (FWI), a set of methods with the capacity to produce high-resolution subsurface models (Tarantola, 1986; Brossier et al., 2009; Virieux and Operto, 2009). FWI, although more computationally intensive, in principle accounts for all of these wave propagation effects, and high resolution elastic parameter models derived from FWI can be directly linked to reservoir properties. FWI therefore appears to be a potentially powerful tool for quantitative CO_2 characterization and monitoring.

In CO_2 applications, rock properties are typically extracted sequentially, with the seismic inversion process geared towards determination of elastic properties, from which the actual properties of interest are subsequently determined, often qualitatively (Johnston, 2013; Zhang et al., 2013; Asnaashari et al., 2015). Queißer and Singh (2013a) applied elastic FWI to the Sleipner time-lapse seismic data, and correlated velocity changes with CO_2 saturation changes using the Gassmann's equations; also at Sleipner, Dupuy et al. (2021) combined acoustic FWI and rock physics inversion to estimate rock frame properties from baseline data and CO_2 saturation from monitor data. However, reports of quantitative, waveform-based CO_2 saturation predictions are uncommon.

The sequential approach itself is neither a necessary, nor always optimal, strategy. The estimation of reservoir properties directly from the seismic data (as opposed to serially, after elastic parameters are first estimated) has several advantages, the main one being that it involves an integrated wave propagation and rock physics formulation, maintaining consistency between elastic and reservoir properties (Doyen, 2007; Bosch et al., 2010). Inversions of this type can be found in seismic amplitude variation with offset (AVO) settings (Spikes et al., 2007; Grude et al., 2013; Grana et al., 2020), but only very recently have FWI formulations in this mode been examined. Hu et al. (2021) formulated a direct procedure for updating rock and fluid properties within elastic FWI. This was achieved by re-parameterizing the inversion in terms of rock physics properties, adopting a viewpoint similar to that of Russell et al. (2011) within an AVO environment. Hu and Innanen (2021) extended the approach to incorporate prior model information.

We have applied the method of Hu et al. (2021) to the problem of CO_2 saturation prediction from time-lapse seismic data. To set out the results of these tests, we first review the rock physics FWI framework within which direct rock property updates are calculated. We then systematically examine the response of the inversion to synthetic time-lapse data generated from the Johansen model from offshore Norway (Grana et al., 2020). Specifically, we recover porosity and clay content from the baseline seismic data, and then use these results as input in the monitor seismic survey, producing estimates of CO_2 saturation. The reliability of the approach is quantified by examining how errors in baseline model estimates and the errors in monitor data affect CO_2 saturation reconstructions. We end by discussing inversion strategies to improve the saturation predictions.

METHODOLOGY

Elastic FWI with rock-physics parameterizations

The FWI algorithm we apply is an outgrowth of that set out by Hu and Innanen (2021), which in turn is based on the frequency-domain inversion formulation of Keating and Innanen (2020). We consider isotropic elasticity and a 2D medium. In the frequency domain, the elastic wave equations can be discretized using the finite difference equations, which take the form

$$\mathbf{Au} = \mathbf{f}, \tag{1}$$

where the coefficients of the impedance matrix $\mathbf{A}$ depend on the frequency and the medium properties, $\mathbf{u}$ is the displacement vector and $\mathbf{f}$ is the body force vector. The coefficients within $\mathbf{A}$ are determined by iteratively minimizing the differences between seismic observations $\mathbf{d}_{\text{obs}}$, and simulation of data $\mathbf{d}_{\text{syn}}$ within model $\mathbf{m}$. The objective function to be minimized is

$$E(\mathbf{m}) = \frac{1}{2}\Delta\mathbf{d}^t\Delta\mathbf{d}^*, \tag{2}$$

where $\Delta\mathbf{d} = \mathbf{d}_{\text{obs}} - \mathbf{d}_{\text{syn}}$ contain the data residuals, and the superscripts ^{t} and * denote the transpose and the complex conjugate, respectively. The gradient of E with respect to the ith model variable m_i is

$$\nabla_{m_i} E = \Re\left\{\mathbf{u}^t\left(\frac{\partial\mathbf{A}}{\partial m_i}\right)^t(\mathbf{A}^{-1})^t\Delta\mathbf{d}^*\right\}. \tag{3}$$

where $\Re$ takes the real part of its argument. Within a Newton optimization, the search direction $\delta\mathbf{m}$ for model update is the solution of

$$\mathbf{H}\,\delta\mathbf{m} = -\nabla_{\mathbf{m}}E, \tag{4}$$

where $\mathbf{H}$ is the Hessian operator. We employ a truncated Gauss Newton method (Métivier et al., 2017), in which equation (4) is solved iteratively, involving only Hessian-vector products.

Let $\mathbf{m} = [m^1, m^2, m^3]$ represent a reference FWI parameterization which is based on three elastic parameters (e.g., the P- and S-wave velocities plus density) and $\mathbf{r} = [r^1, r^2, ..., r^n]$ represent a desired FWI parameterization based on n different rock physics properties, we can express the elastic variables at the i^{th} spatial position as a function of the rock physics variables at the same position: $(m_i^1, m_i^2, m_i^3) = g(r_i^1, r_i^2, ..., r_i^n)$, where g is the rock physics model. From equation (3), we observe that the elastic variables are altered at each iteration by an update proportional to $\partial\mathbf{A}/m_i$. To transform to the new parameterization $\mathbf{r}$, we compute the chain rule

$$\frac{\partial\mathbf{A}}{\partial r_i^j} = \frac{\partial\mathbf{A}}{\partial m_i^1}\frac{\partial m_i^1}{\partial r_i^j} + \frac{\partial\mathbf{A}}{\partial m_i^2}\frac{\partial m_i^2}{\partial r_i^j} + \frac{\partial\mathbf{A}}{\partial m_i^3}\frac{\partial m_i^3}{\partial r_i^j}, \tag{5}$$

for each of $j = (1, 2, ..., n)$. Given a conventional FWI scheme set up to update variables $\mathbf{m}$, within which the partial derivatives of $\mathbf{A}$ are known, and given the rock physics model g, so that the partial derivatives of $\mathbf{m}$ with respect to $\mathbf{r}$ can be derived, through equation (5) we can move to a new scheme in which the $\mathbf{r}$ are updated.

We examine a classic rock physics model: the stiff-sand model, which is widely applied to sand and shale formations (Spikes et al., 2007; Grana, 2016; Wawrzyniak-Guz, 2019). We assume two mineral components, quartz and clay, and two fluid components, water and CO_2. Hence, we define three model unknowns: porosity (ϕ), clay content (C), and CO_2 saturation (Sc). The partial derivatives of velocities and density with respect to $\mathbf{r} = [\phi, C, Sc]$ can be calculated numerically.

Time-lapse FWI

CO_2 monitoring requires accurate and precise predictions of the CO_2 saturation model at any time at which the data are measured. Although it is possible to jointly invert the three variables from a single seismic survey, preliminary tests showed that fluid saturation is very difficult to estimate within this parameterization. Here we make two assumptions: 1) before CO_2 injection, there is only one fluid component (water) in the subsurface; 2) ϕ and C are constant in time. Therefore, we propose to estimate the three variables sequentially: First, we apply the rock physics FWI approach to estimate ϕ and C from baseline (pre-injection) data; then, we use the same inverse method and use the recovered baseline model as input to estimate Sc from monitor (post-injection) data. The objective function for baseline model reconstruction is expressed as

$$E_b = \left\|\mathbf{d}_{\text{obs\_b}}(\phi^t, C^t) - \mathbf{d}_{\text{syn\_b}}(\phi, C)\right\|^2, \tag{6}$$

where $\mathbf{d}_{\text{obs\_b}}$ and $\mathbf{d}_{\text{syn\_b}}$ denote the observed and synthetic baseline data, respectively. ϕ^t and C^t denote the true porosity and clay content models. The objective function for monitor model reconstruction is

$$E_m = \left\|\mathbf{d}_{\text{obs\_m}}(\phi^t, C^t, S^t_{c\_m}) - \mathbf{d}_{\text{syn\_m}}(\phi_{\text{inv}}, C_{\text{inv}}, S_{c\_m})\right\|^2, \tag{7}$$

where $\mathbf{d}_{\text{obs\_m}}$ and $\mathbf{d}_{\text{syn\_m}}$ are the observed and synthetic monitor data, respectively. ϕ_{inv} and C_{inv} are the inverted porosity and clay content models from the baseline survey. S_{c_m} is the CO_2 saturation model to estiamte.

NUMERICAL EXAMPLES

We apply the proposed approach to a CO_2 sequestration study based on the Johansen formation model. Physical properties including porosity and permeability of this model are available (Eigestad et al., 2009; Bergmo et al., 2011). The original geo-cellular model is discretized in $100 \times 100 \times 5$ cells, however, we consider 100×5 cells defined on an irregular gird in the vertical direction (Figure 1a). The initial water saturation (before injection) is equal to 1 everywhere. The CO_2 saturation distribution in Figure 1b is calculated by simulating the fluid flow in year 110 (Grana et al., 2020).

We make several changes to the model in Figure 1. First, we define a regular grid and interpolate the scattered data over the grid; second, we modify the coordinates using relative depth and position. Moreover, we introduce a clay volume with negative linear correlation with porosity. The reservoir models in Figures 2a, 2b, and 3a are then generated to examine the proposed method. In the numerical experiments, the data are computed with the same algorithm for observed and synthetic data in inversion. We use an acquisition geometry with receivers mimicking a simultaneous surface seismic and vertical

seismic profile configuration: a line of sources at the top of the model illuminates receivers on the top and sides of the model.

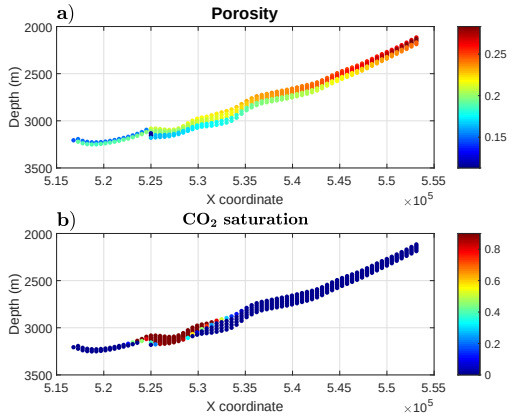

Figure 1: True reservoir model of the Johansen formation: (a) Porosity. (b) CO_2 saturation distribution in year 110.

Baseline model reconstruction

For the initial porosity model, we filter the true model of P-wave velocity and apply a linear regression for porosity. The low frequency model of velocity is often related to models used for seismic processing, for example stacking velocities. The initial clay model is computed from porosity based on the exact relationship between them. The signal-to-noise ratio (SNR) of the data is assumed to be 10. We adopt the regularization strategy of Hu and Innanen (2021) to enforce explicit physical relationships between the updated variables. The recovered porosity and clay content models are resonably accurate (Figure 2e and 2f).

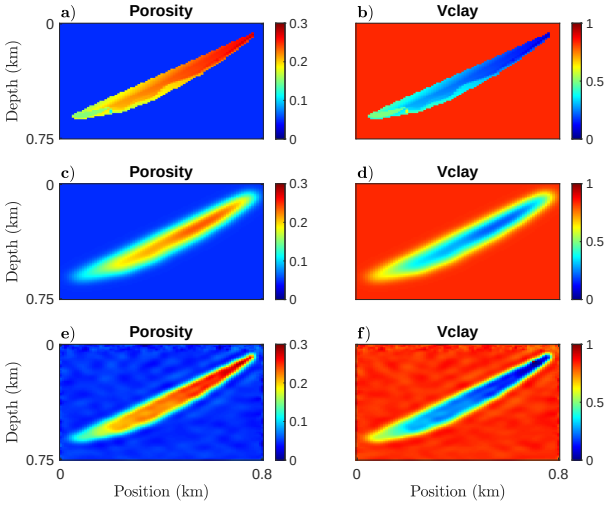

Figure 2: (a,b) True, (c,d) initial, and inverted (e,f) models of porosity and clay content.

Monitor model reconstruction

In the monitor survey, the observed data is generated from the true porosity, clay content, and CO_2 saturation models; the synthetic data is generated from the porosity and clay models estimated from the basline survey plus the current estimate of CO_2 saturation. For the intial guess of the CO_2 saturation distribution, we assume that the plume had migrated 20 traces to the left and 20 traces to the right, within the reservoir, at the time the monitor data were acquired (Figure 3b).

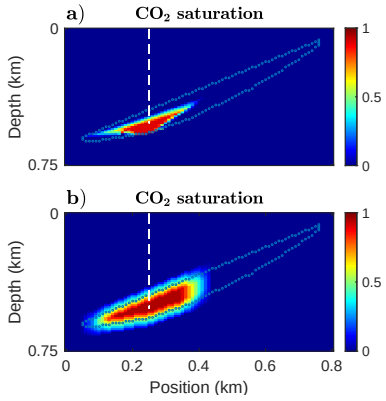

Figure 3: (a) True and (b) initial CO_2 saturation models. The white dashed line denotes the location of the injection well. The blue dashed line denotes the reservoir boundary.

We first carry out noise-free tests to examine the impact of baseline model estimates. Three cases are considered: the baseline model is poorly, properly, and perfectly resolved. For this, we use the initial model in Figure 2c and 2d, the inverted model in Figure 2e and 2f, and the true model in Figure 2a and 2b, respectively, as input. The results are plotted in Figure 4. For the case of poor baseline model, we can clearly observe the effect known as parameter crosstalk, i.e., errors in the baseline model are mapped to the updates of CO_2 saturation (Figure 4a). With proper baseline model, the saturation model is recovered to some extent, with the shape of the plume slightly distorted and the parameter values slightly overestimated (Figure 4b). These can be interpretated as a consequence of erroneous baseline model input, if using the case of perfect baseline model as a reference (Figure 4c).

Next we repeat the experiment in Figure 4b to examine random noise effects. We add white Gaussian noise to the data considering three noise levels: signal-to-noise ratio are 20, 10, and 5. Compared to the noise-free case, the recovered models are contaminated by artifacts more seriously (Figure 5a-5c). In the cases with moderate and strong noise (SNR=10 and 5), the plume behavior is undesirable, with CO_2 patchily distributed over large areas.

The results suggest that CO_2 saturation is very sensitive to data errors. This likely originates from the small impact of CO_2 saturation on elastic parameters. To stabilize the inversion, we consider the first-order Tikhonov regularization, which is based on the assumption that neighboring points in the model should be close in value, leading to smooth solutions (Tikhonov and Arsenin, 1977). We use a fixed hyper-parameter and choose its value such that the ratio between the model penalty and data misfit terms is 5×10^{-3} at the first iteration, following

the strategy advocated by Asnaashari et al. (2013). We repeat the experiments in Figure 5a-5c using the regularized scheme and plot the results in Figure 5d-5f. Large discontinuities are preserved while small ones are pushed toward zero, leading to estimates that match more closely the true model.

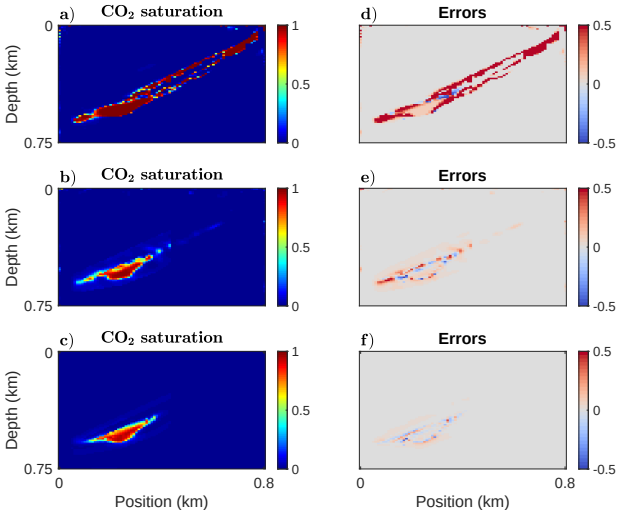

Figure 4: Inversion test to examine the impact of baseline model estimates on monitor model reconstruction. (a-c) The recovered CO_2 saturation models and (d-f) the corresponding model errors.

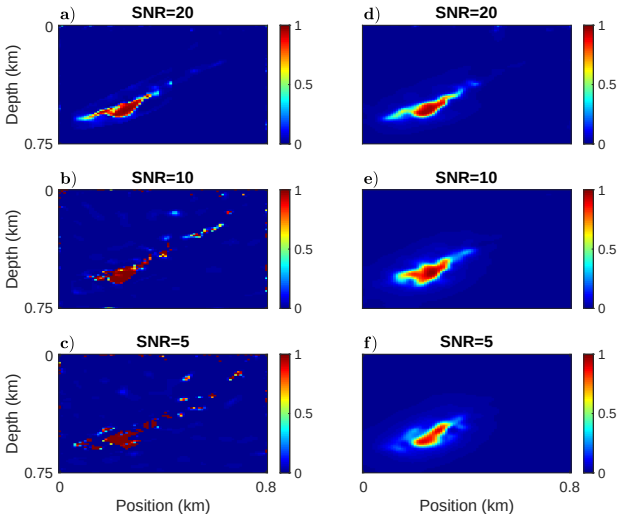

Figure 5: Inversion test to examine random noise effects, using the inverted baseline model (Figs 2c and d) as input. (a-c) Recovered CO_2 saturation models with a signal-to-noise ratio of 20, 10, and 5, respectively. (d-f) Repeat (a-c) using smoothness constraint.

In Figure 6, we compare the convergence properties of the solutions among four experiments that we have previously carried out. We use the model error $e = \|\mathbf{m} - \mathbf{m}_t\|_2 / \|\mathbf{m}_0 - \mathbf{m}_t\|_2$, where $\mathbf{m}$, $\mathbf{m}_0$, and $\mathbf{m}_t$ represent the inverted, initial and true models, respectively. We observe that the combined uncertainty (uncertainties in baseline model and monitor data) causes large and sustained increases in model error, especially at later stages after the introduction of higher frequency data. Comparing this to the evolution of the model error with the smoothness constraint, the convergence characteristics of a reliable inversion is retained.

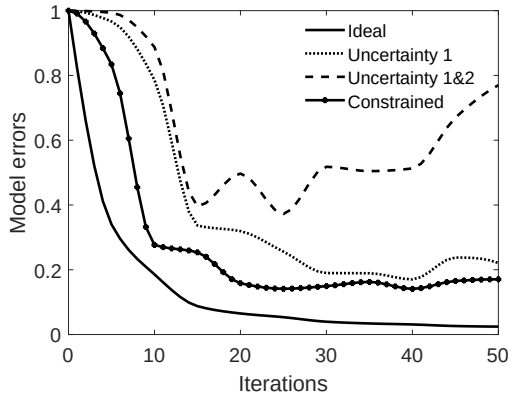

Figure 6: Model error reductions of CO_2 saturation in different experiments. Solid line: perfect baseline model and noise-free monitor data (Figure 4c). Dotted line: proper baseline model and noise-free monitor data (Figure 4b). Dashed line: proper baseline model and noisy data (Figure 5b). Solid line with markers: with smoothness constraint (Figure 5e).

CONCLUSION

We present a quantitative CO_2 monitoring approach which is based on seismic FWI. Unlike conventional FWI approaches which aim at determination of elastic properties, the proposed scheme allows direct prediction of rock physics properties from seismic data. The method was validated on synthetic data generated for the Johansen formation model. The inversion results show high prediction accuracy for baseline porosity and clay content models but seriously harmful effects of the uncertainties in baseline model and monitor data on the predicted CO_2 saturation. We show that it is recommended to impose smoothness on the solution to mitigate undesired discontinuities and to obtain meaningful CO_2 saturation distributions. The proposed methodology was applied to a deep saline aquifer but could be extended to depleted hydrocarbon reservoirs as well as enhanced oil recovery and carbon capture, utilization, and storage (CCUS) applications.

ACKNOWLEDGMENTS

This work was funded by CREWES industrial sponsors and NSERC (Natural Science and Engineering Research Council of Canada) through the grant CRDPJ 543578-19. The first author was partially supported by a scholarship from the SEG Foundation.

REFERENCES

Alemie, W. M., 2017, Time-lapse full waveform inversion methods: PhD thesis, Alberta University.

Asnaashari, A., R. Brossier, S. Garambois, F. Audebert, P. Thore, and J. Virieux, 2013, Regularized seismic full waveform inversion with prior model information: Geophysics, **78**, no. 2, R25–R36.

———, 2015, Time-lapse seismic imaging using regularized full-waveform inversion with a prior model: which strategy?: Geophysical prospecting, **63**, 78–98.

Bergmo, P. E. S., A.-A. Grimstad, and E. Lindeberg, 2011, Simultaneous CO_2 injection and water production to optimise aquifer storage capacity: International Journal of Greenhouse Gas Control, **5**, 555–564.

Bosch, M., T. Mukerji, and E. F. Gonzalez, 2010, Seismic inversion for reservoir properties combining statistical rock physics and geostatistics: A review: Geophysics, **75**, no. 5, 75A165–75A176.

Brossier, R., S. Operto, and J. Virieux, 2009, Seismic imaging of complex onshore structures by 2D elastic frequency-domain full-waveform inversion: Geophysics, **74**, no. 6, WCC105–WCC118.

Davis, T. L., M. Landrø, and M. Wilson, 2019, Geophysics and geosequestration: Cambridge University Press.

Doyen, P., 2007, Seismic reservoir characterization: An earth modelling perspective: EAGE publications.

Dupuy, B., A. Romdhane, P. Eliasson, and H. Yan, 2021, Combined geophysical and rock physics workflow for quantitative CO_2 monitoring: International Journal of Greenhouse Gas Control, **106**, 103217.

Eigestad, G. T., H. K. Dahle, B. Hellevang, F. Riis, W. T. Johansen, and E. Øian, 2009, Geological modeling and simulation of CO_2 injection in the Johansen formation: Computational Geosciences, **13**, 435.

Ghosh, R., M. K. Sen, and N. Vedanti, 2015, Quantitative interpretation of CO_2 plume from Sleipner (North Sea), using post-stack inversion and rock physics modeling: International journal of greenhouse gas control, **32**, 147–158.

Grana, D., 2016, Bayesian linearized rock-physics inversion: Geophysics, **81**, no. 6, D625–D641.

Grana, D., M. Liu, and M. Ayani, 2020, Prediction of CO_2 saturation spatial distribution using geostatistical inversion of time-lapse geophysical data: IEEE Transactions on Geoscience and Remote Sensing, **59**, 3846–3856.

Grude, S., M. Landrø, and B. Osdal, 2013, Time-lapse pressure–saturation discrimination for CO_2 storage at the Snøhvit field: International Journal of Greenhouse Gas Control, **19**, 369–378.

Hu, Q., and K. Innanen, 2021, Elastic full-waveform inversion with rock-physics constraints: First International Meeting for Applied Geoscience & Energy, Society of Exploration Geophysicists, 662–666.

Hu, Q., S. Keating, K. A. Innanen, and H. Chen, 2021, Direct updating of rock-physics properties using elastic full-waveform inversion: Geophysics, **86**, no. 3, MR117–MR132.

Johnston, D. H., 2013, Practical applications of time-lapse seismic data: Society of Exploration Geophysicists.

Keating, S., and K. A. Innanen, 2020, Parameter crosstalk and leakage between spatially separated unknowns in viscoelastic full-waveform inversion: Geophysics, **85**, no. 4, R397–R408.

Métivier, L., R. Brossier, S. Operto, and J. Virieux, 2017, Full waveform inversion and the truncated Newton method: SIAM Review, **59**, 153–195.

Queißer, M., and S. C. Singh, 2013a, Full waveform inversion in the time lapse mode applied to CO_2 storage at Sleipner: Geophysical prospecting, **61**, 537–555.

———, 2013b, Localizing CO_2 at Sleipner-seismic images versus P-wave velocities from waveform inversion: Geophysics, **78**, no. 3, B131–B146.

Ringrose, P., 2020, How to store CO_2 underground: insights from early-mover ccs projects: Springer.

Russell, B. H., D. Gray, and D. P. Hampson, 2011, Linearized AVO and poroelasticity: Geophysics, **76**, no.3, C19–C29.

Spikes, K., T. Mukerji, J. Dvorkin, and G. Mavko, 2007, Probabilistic seismic inversion based on rock-physics models: Geophysics, **72**, no. 5, R87–R97.

Tarantola, A., 1986, A strategy for nonlinear elastic inversion of seismic reflection data: Geophysics, **51**, no. 10, 1893–1903.

Tikhonov, A. N., and V. Y. Arsenin, 1977, Solutions of ill-posed problems: Winston and Sons.

Virieux, J., and S. Operto, 2009, An overview of full-waveform inversion in exploration geophysics: Geophysics, **74**, no. 6, WCC1–WCC26.

Wawrzyniak-Guz, K., 2019, Rock physics modelling for determination of effective elastic properties of the lower Paleozoic shale formation, North Poland: Acta Geophysica, **67**, 1967–1989.

Zhang, F., C. Juhlin, M. Ivandic, and S. Lüth, 2013, Application of seismic full waveform inversion to monitor CO_2 injection: Modelling and a real data example from the Ketzin site, Germany: Geophysical Prospecting, **61**, 284–299.